Contents lists available at ScienceDirect

Quaternary Science Reviews

journal homepage: www.elsevier.com

Using differential structure-from-motion photogrammetry to quantify erosion at the Engare Sero footprint site, Tanzania

Brian Zimmer[a, *], Cynthia Liutkus-Pierce[a], Scott T. Marshall[a], Kevin G. Hatala[b], Adam Metallo[c], Vincent Rossi[c]

[a] Department of Geological and Environmental Sciences, Appalachian State University, 572 Rivers St, Boone, NC, USA
[b] Department of Biology, Chatham University, Woodland Rd, Pittsburgh, PA, USA
[c] Digitization Program Office, Smithsonian Institution, 600 Maryland Avenue, SW, Suite 810W, Washington, D.C., USA

ARTICLE INFO

Article history:
Received 26 April 2018
Received in revised form 3 July 2018
Accepted 4 July 2018
Available online xxx

Keywords:
Structure-from-Motion
Differential structure from motion
Photogrammetry
Present
Landscape evolution
East Africa
Footprint
Engare Sero
Change detection
Conservation
M3C2
Erosion

ABSTRACT

Hominin footprint sites are excellent sources of data that provide insights into early human physiology, anatomy, and social structures. They are also potential tourist attractions that are often situated in relatively under-developed parts of the world. Unfortunately, many footprint sites are also located in high energy environments and/or are pressed into poorly indurated sediments, which make them highly susceptible to erosion. This paper proposes a non-invasive and low-cost method employing Structure-from-Motion photogrammetry to quantify erosion rates in the absence of permanent ground control points. Using point cloud comparison algorithms between data collected at different times, it is possible to quantitatively analyze the locations, volumes, and rates of material loss. We applied this technique to several footprints within the Engare Sero footprint site in northern Tanzania to assess erosional change between 2010 and 2017. Our comparisons show that prints are vertically eroding at average rates ranging from 0.11 to 0.17 mm/yr with some localized areas experiencing much higher rates over shorter durations. We identify three primary modes of erosion: 1) flaking, 2) abrasion, and 3) boring of holes. Erosion appears to have occurred episodically with major events, such as flooding, separated by periods of relative stability. The methods presented here are valuable for paleoanthropologists to better understand how footprint erosion might adversely affect inferences regarding print-makers, and they are valuable for decision-makers, who can create conservation plans to better protect and maximize the utility of known hominin footprint sites.

1. Introduction

1.1. Importance of human track sites

Vertebrate tracks are often ephemeral, but under exceptional circumstances these traces may become part of the fossil record. When preserved, these ichnological data can provide avenues for important paleobiological insights regarding extinct taxa, including those related to anatomy, locomotion, social behaviors, and paleoenvironments (see Falkingham, 2014 for a review).

The record of tracks known from fossil hominins has been historically less robust than the ichnological records of some other fossil groups (e.g., dinosaurs) but the potential richness of the inferences that can be derived from hominin tracks has long been recognized. For example, immediately following the discovery of the 3.66 Ma hominin footprints at Laetoli (Leakey and Hay, 1979), analyses of these data were used to infer aspects of foot anatomy and locomotion (e.g., Day and Wickens, 1980; White, 1980; Charteris et al., 1981, 1982; Stern and Susman, 1983), social interactions (Leakey and Hay, 1979; Leakey, 1981), and the paleoenvironmental and depositional contexts (Leakey and Hay, 1979; Leakey, 1981).

More recently, new analytical methods have been developed and applied to reassess previously known hominin tracks (e.g., analyses of Laetoli tracks by Berge et al., 2006; Raichlen et al., 2010; Crompton et al., 2012; Hatala et al., 2016a), but a relative influx in hominin footprint discoveries over the past decade has provided new data and new questions regarding our evolutionary past. For instance, newly discovered 3.66 Ma trackways at Laetoli have revealed a higher level of size variation than previously recognized, which has implications for social behavior (Masao et al., 2016). Discoveries and subsequent analyses of 1.5 Ma footprints near Ileret, Kenya that are provisionally attributed to *Homo erectus* have suggested modern human-like patterns of foot anatomy and locomotion (Bennett et al., 2009; Hatala et al., 2016b), human-like social structures (Hatala et al., 2016b), and intensive use of lake margin habitats (Roach et al., 2016). Footprints dating to 1.0–0.78 Ma at Happisburgh, UK offer unique evidence of hominin occupation of northern Europe during the Early Pleistocene (Ashton et al., 2014). The co-occurrence of stone artifacts and hominin footprints on a 0.7 Ma surface at Melka Kunture, Ethiopia provides a rich record from which to infer behavioral patterns with different lines of synchronous data (Altamura et al., 2016). Sets of 10–16 ka tracks that were recently discovered in New Mexico, USA may directly record hunting behaviors of late

* Corresponding author.
Email address: zimmerbw@appstate.edu (B. Zimmer)

https://doi.org/10.1016/j.quascirev.2018.07.006
0277-3791/

Pleistocene humans (Bustos et al., 2018). These and other recent discoveries of human track sites have greatly expanded our knowledge of aspects of our evolutionary past. As the hominin track record continues to grow, methods to analyze them are sure to simultaneously expand, and more long-standing questions are likely to be addressed.

In addition to the scientific utilities listed above, footprint sites can also potentially increase tourism to otherwise undervisited regions of the world. Preservation infrastructure at footprint sites varies depending on the size and stability of a site as well as the tourism potential and financial resources available for development. Many localities have little more than an interpretive sign to indicate the location of a footprint site while others have pavilion structures, protected pits, and full museum displays on site (Lofgren et al., 2006; Roberts, 2008; Schmincke et al., 2009; Bennett et al., 2013). A balance must be reached between the scientific, cultural, and economic significance of a particular site and the expenditure of resources required to protect and develop it.

For both scientific inquiry and tourism potential, footprint sites must be considered a resource; one that is finite and, unfortunately, not permanent. Trackways are highly susceptible to erosion because they are often preserved in relatively soft and/or fine-grained sediments (e.g., Behrensmeyer and Laporte, 1981; Ashley and Liutkus, 2002). While the number of documented trackway sites has increased in the last several decades, some footprint sites have degraded (or been permanently lost) due to wind and rain (Marty et al., 2009; Bennett et al., 2013) or exposure to intense coastal erosion, where the prints only lasted a number of weeks (e.g. Formby Point, UK; Wiseman and De Groote, 2018, Happisburgh, UK; Ashton et al., 2014). Human-generated erosion through repeated excavation, vandalism, careless driving, and foot traffic has also been noted (Morgan et al., 2007; Bennett et al., 2013). Despite the most well-intentioned preservation efforts, sites of significant scientific and cultural importance have nonetheless degraded significantly through time (e.g., Laetoli, Tanzania; Demas and Agnew, 2006; Dalton, 2008). This degradation is of further import because many of the aforementioned paleobiological inferences derived from hominin footprints have relied in some way upon predictions of body size from footprint size. These inferences are therefore inherently tied to assumptions that footprint sizes are reliable records of true foot sizes. The integrity of this record, and the range of paleobiological questions to which footprint data can be applied, will diminish as footprints progressively erode and lose resolution (Wiseman and De Groote, 2018). There is clearly a desire to preserve footprints sites for scientific investigations, for cultural heritage reasons, and for potential economic development, but preservation is not always economically feasible and in some cases, not even possible. In many cases, the best option for long-term preservation may be digital curation.

1.2. Applications of SfM

With recent improvements in computing power and rendering software, it has become simpler and more expedient than ever to construct three-dimensional digital models of real-world objects and features using various Structure-from-Motion (SfM) algorithms (e.g. Luhmann et al., 2013; Mallison and Wings, 2014; Matthews et al., 2016; James et al., 2017). SfM is the process of rendering three-dimensional digital models from a series of overlapping images taken from different viewpoints. SfM produces three-dimensional models that allow for accurate and detailed quantitative measurements (Matthews, 2008; Bemis et al., 2014; Mallison and Wings, 2014). Furthermore, SfM models can be easily disseminated and archived as well as remotely manipulated and quantitatively analyzed. Historically, these models were simply nice visualizations. Today, however, with improved digital cameras and photogrammetric techniques, model resolution can be refined enough to make accurate measurements at the sub-mm-scale (Bemis et al., 2014). Current applications of SfM photogrammetry include, but are not limited to, estimating landslide volumes (e.g., Lucieer et al., 2013; Stumpf et al., 2015), monitoring active river systems (e.g., Javernick et al., 2014; Marteau et al., 2017), assessing cliff morphology (e.g., Ružić et al., 2014; Warrick et al., 2017), assessing large-scale erosion at recreation sites (e.g., Matthews, 2008) and measuring earthquake rupture zones and fault structures (e.g., Johnson et al., 2014). Here, we utilize differential SfM photogrammetry to quantify the rates and spatial patterns of erosion that are occurring at a hominin footprint site of archaeological and paleoanthropological importance.

The use of SfM photogrammetry to digitally preserve and distribute footprint morphological data has previously been applied to both human (Rüther et al., 2012; Bennett et al., 2016; Citton et al., 2017; Helm et al., 2018) and dinosaur track sites (Matthews et al., 2006; Petti et al., 2008; Pond et al., 2014; Citton et al., 2015; Marty et al., 2017; Belvedere et al., 2018). Furthermore, Adams et al., (2010) demonstrated that erosion detection could, hypothetically, be performed on footprint sites using a hand-held laser scanner. While these studies used SfM photogrammetry for documentation and visualization of footprint sites, at the time of writing, no studies have thus far used differential SfM-based analyses over time to assess actual rates of change at trackway sites.

In addition to the loss of a potential tourist attraction, erosion of footprints can influence morphometric measurements made to estimate the stature and kinematics of print-makers (Wiseman and DeGroote, 2018). In this paper, we use SfM photogrammetry to quantify the rate of erosional degradation at the Engare Sero footprint site. The methods used here can provide quantitative data to improve methods for paleoanthropological inferences and assist in the creation of appropriate conservation plans.

2. Regional setting

Our research locality, the Engare Sero footprint site, is located in northern Tanzania, on the southern shore of Lake Natron (Fig. 1). Lake Natron sits just north of the Natron-Engaruka explosion crater area, which is bound on the west by the East African Rift escarpment and on the east by the extinct shield volcano, Gelai (Dawson and Powell, 1969; Dawson, 2008). Due to extension along the rift and associated crustal thinning since the Pliocene, the region is volcanically active (Bosworth, 1987; Dawson, 1992). Volcanic features within this region vary dramatically in size, age, and composition ranging from Pliocene shield volcanoes (e.g., Gelai) to intermediate composite volcanoes that are carbonatitic in composition (e.g., Oldoinyo L'engai; Dawson, 1962) to smaller tuff cones, rings, and explosion craters (e.g., Loolmurwak Crater; Dawson, 2008).

Both human and animal tracks have been identified at Engare Sero, scattered over an area covering several km^2 (Liutkus-Pierce et al., 2016). The surface that hosts the human tracks is a 250 m^2, NE-SW trending exposure of volcaniclastic deposits that sits in an ephemeral channel of the Engare Sero River (Fig. 2). To the south, the river channel has eroded most of the foot-printed surface. However, to the north, sand dunes composed primarily of olivine and hornblende eroded from nearby volcanic centers cover the site. The human footprint trackways begin approximately 20 m south of the dune line and continue northeast up to and beneath the dunes. Several fossil zebra and buffalo trackways are located approximately 30 m SW of the human footprint site toward the ephemeral Engare Sero

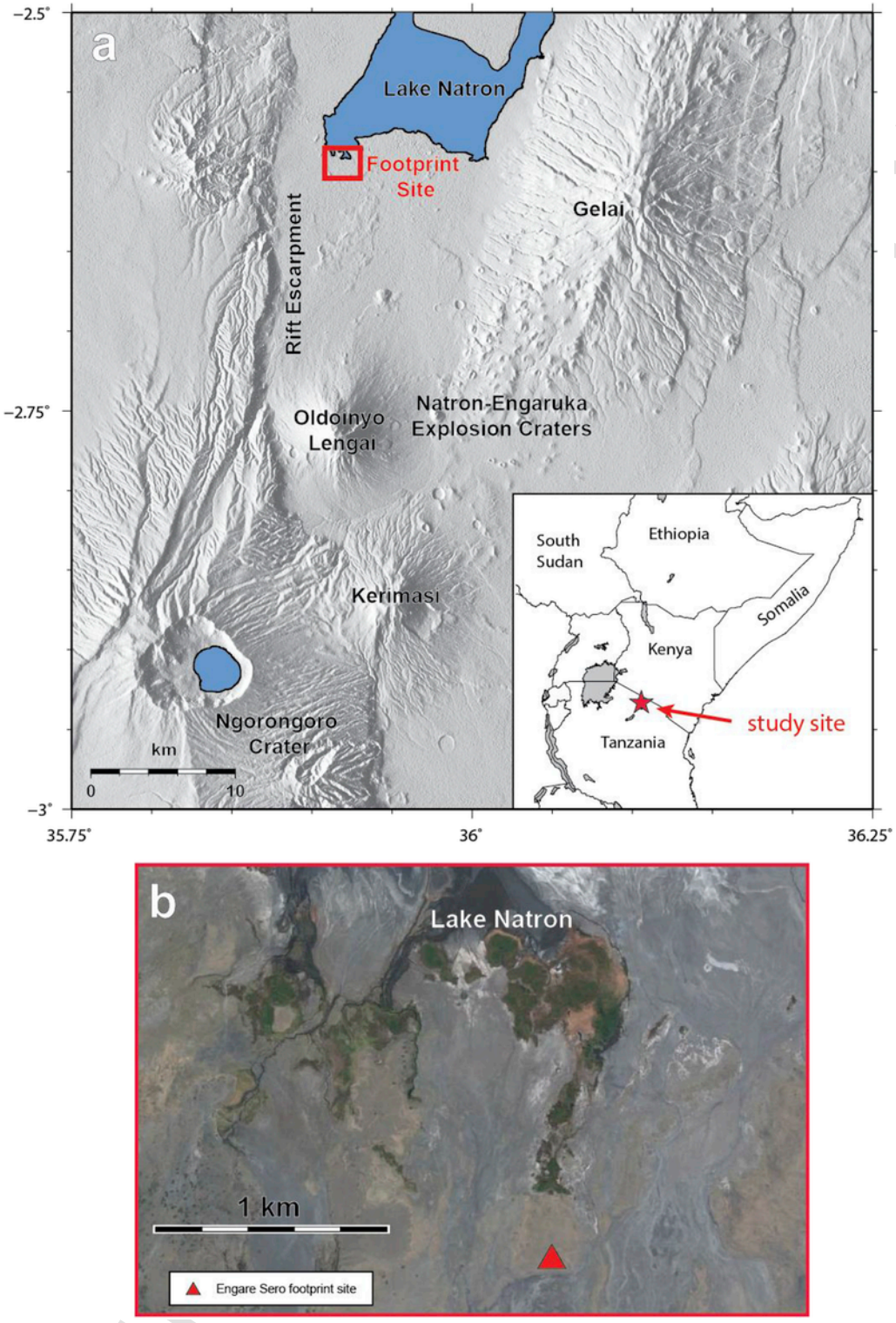

Fig. 1. a) Regional setting of the Engare Sero footprint site along the south shore of Lake Natron in northern Tanzania. Prominent regional volcanic centers are labeled. The red box indicates the location of part b). b) Google Earth imagery of the study site showing the footprint locality in proximity to local springs and drainages (green vegetated areas) feeding Lake Natron. Figure is adapted from Liutkus-Pierce et al. (2016). (For interpretation of the references to colour in this figure legend, the reader is referred to the Web version of this article.)

Fig. 2. The Engare Sero footprint site (looking south), as it appeared in 2010. The prominent edifice in the background is the stratovolcano Oldoinyo L'engai, bounded to the west by the rift escarpment. In 2010, only a small cobble border denoted the boundary of the site. Non-vegetated areas are part of the Engare Sero River channel that floods periodically. Figure adapted from Liutkus-Pierce et al. (2016).

River channel, and several other sites containing animal footprints are greater than 1 km to the northwest (Liutkus-Pierce et al., 2016).

The Engare Sero footprint site comprises over 400 fossilized tracks of *Homo sapiens* that are dated to a range of 5760 (±30) to 19,100 (±3100) ybp (Liutkus-Pierce et al., 2016). At the time of formation, the tracks were pressed into fine-grained volcaniclastic sediments along the southern shoreline of paleo-Lake Natron. Ultimately, preservation occurred when the tracks were inundated by a low-energy lahar transporting ash that was primarily produced by the nearby volcano, Oldoinyo L'engai (Liutkus-Pierce et al., 2016). Subsequent cementation of the sediment hardened the surface to its current state (Fig. 2).

The trackway site was originally discovered in 2006 (Liutkus-Pierce et al. (2016)) and geologic field surveys and excavations occurred during summer field seasons in 2009, 2010, 2011, 2012, and 2017. The majority of the tracks at the site were uncovered during the 2010 field season. Additional tracks are likely preserved beneath a sand dune immediately adjacent to the current exposure (Fig. 2) and could become exposed as the overlying sediments erode away or through further excavation.

3. Overview of three-dimensional imaging techniques

The purpose of this study is to quantify the rates and spatial distribution of erosion at the Engare Sero footprint site through three-dimensional analyses of the foot-printed surface. There are currently two commonly used methods for producing three-dimensional models of surficial geologic features; laser-scanning (i.e., LiDAR) and SfM photogrammetry. Below, we briefly outline the strengths and drawbacks of each method.

3.1. LiDAR-based methods

High-quality digital elevation data can be collected through orbital, airborne, or terrestrial Light Detection And Ranging (LiDAR) methods (Carrivick et al., 2016; Fey and Wichmann, 2017). While orbital and airborne LiDAR provide exceptional results over relatively large areas (m to km-scale, useful for landscape reconstructions), they are expensive to collect and unable to provide the resolution necessary when investigating small-scale (<1 m) features (Johnson et al., 2014). Airborne Laser Scanning (ALS) using drones is rapidly improving with new deployment options available, but ALS devices and the drones required to fly them are still large and expensive (Johnson et al., 2014). Terrestrial Laser Scanners (TLS) that are capable of imaging outcrop-scale features can also be used to image sub-meter features, however in sites with significant topography, occlusion of data due to a loss of line-of-sight can result in suboptimal products (Lague et al., 2013). For footprint-scale targets, where point densities on the sub-mm-scale are required, a hand-held laser-scanning device may be necessary. Hand-held laser scanners have successfully documented several footprint sites (e.g. Gonzalez et al., 2006; Bennett et al., 2009; Bennett et al., 2016). Comparative studies have shown that, for many applications, a digital camera and SfM software can replace tens of thousands of dollars' worth of laser scanners while producing data at similar resolution and accuracy (Petti et al., 2008; Falkingham, 2012; Johnson et al., 2014).

3.2. SfM photogrammetry

For this study, we employed SfM photogrammetry instead of laser scanning due to the size of the targets, the cost, the availability of equipment, and the ease of transporting cameras (as opposed to more delicate devices) to a remote locality. An advantage of SfM photogrammetry is that data capture with a camera is less time-intensive than with laser-scanning devices. While using a camera in the field, it is possible to be more mobile and to shoot more targets than would be possible over similar periods of time using TLS or handheld scanners. The tradeoff in time is in the data processing. With most laser scanners, the data return is very quick and the quality of the render is known shortly after the survey. Currently, SfM photogrammetry can require a few hours to days for image processing before a final high-resolution model is produced. The total time required is dependent on the number of photos, resolution of the render produced, and computer hardware used. Most field laptops will allow for preliminary data review, but are, currently, inefficient for rendering full-resolution models. The quality of SfM photogrammetry models decreases

in vegetated landscapes or when shooting highly reflective surfaces (Mallison and Wings, 2014; Carrivick et al., 2016; Matthews et al., 2016). In vegetated landscapes, the visual returns, upon which image alignment software depends, are often noisy due to slight movement of vegetation between shots. Vitreous targets, such as water or glaciers, also have inconsistent returns due to light reflecting back to the camera at different angles. LiDAR is generally able to handle these conditions with greater accuracy (Raber et al., 2002; Kobler et al., 2007; Johannesson et al., 2013).

4. Methods

The Engare Sero footprint site was first photogrammetrically documented in 2010 by members of the Smithsonian 3D digitization program (A.M. and V.R.). At that time, the entire site was photographed using a mobile rigging system that allowed the team to seamlessly stitch the entire site together into a single model. The team also selected several well-developed footprints (H12, I2, R1) to shoot in higher resolution (Fig. 3). The individual prints were photographed again in 2012 and 2017. Footprint R1 is located in the northcentral part of the footprint site, H12 is from the southcentral portion, and I2 is in the northeastern quadrant (Fig. 4). All three prints are situated on slightly raised sections of local topography.

The workflow for the erosional analysis involves five stages: (1) image acquisition in the field, (2) image alignment and three-dimensional model generation using SfM, (3) cloud-to-cloud alignment of three dimensional models from different times, (4) change detection and identification of areas of significant change, and (5) DEM generation and data visualization (Fig. 5).

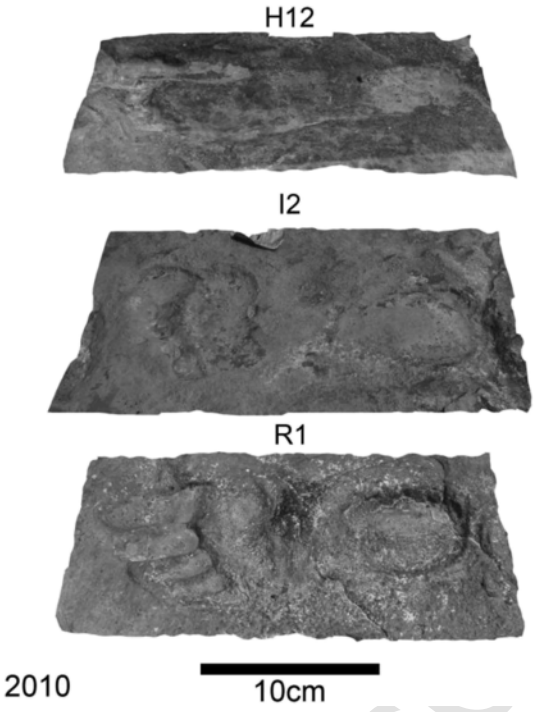

Fig. 3. Oblique views of textured three-dimensional models of the three target footprints for this study. Models are from 2010 imagery. Scale bar is approximate.

4.1. Image acquisition

During the 2010 and 2012 field seasons, images were captured by Canon 5D Mark II DSLR cameras with Canon EF 50 mm prime lenses. The cameras used in 2010 and 2012 were the same model but not the same mounting apparatus. During both of these excursions, scaling was done using a single mm-incremented scale bar running lengthwise parallel to the footprints. In 2017, a Canon Powershot SX60 HS with adjustable lens was used. Scaling was improved in 2017 through the use of three 0.01 mm calibrated scale bars oriented along both the length and width of the print (Fig. 5D, Table 1). Ideally, the same camera, lens, and scales would have been used for all image capture but that was not possible in this case. We made camera selections based on availability as opposed to any technical advantage. Changing cameras, lenses, or scale bars between data sets adds potential sources of error due to differences in resolution and lens distortion (Matthews, 2008; Mallison and Wings, 2014). For example, the Powershot SX used auto-focus, which changed the focal length between each shot; however, this was accounted for when processing the imagery prior to image alignment.

Several papers describe optimized shooting techniques based on the shape and size of the target as well as the algorithm used for image alignment (e.g. Matthews et al., 2006; Falkingham, 2012; Westoby et al., 2012; Wenzel et al., 2013; Mallison and Wings, 2014; Matthews et al., 2016; Falkingham et al., 2018). During the 2010 and 2012 image acquisitions, the footprints were shot primarily from an azimuth perspective as was the recommended method for the 3DM Analyst software package that was employed at that time (www.adamtech.com.au). The azimuth technique shoots straight down on the target with a grid coverage at various levels of zoom. This improves the accuracy of image alignment but the changing focal length must be accounted for by setting up several camera calibration groups while processing the imagery. The azimuth shooting technique is also subject to higher error on vertical and overhanging surfaces due to occlusion (Johnson et al., 2014). Recently, a number of works have demonstrated that better results can be achieved through employing a geometry of converging oblique images to reduce lens distortion, occlusion, and other systemic errors (e.g. Wackrow and Chandler,

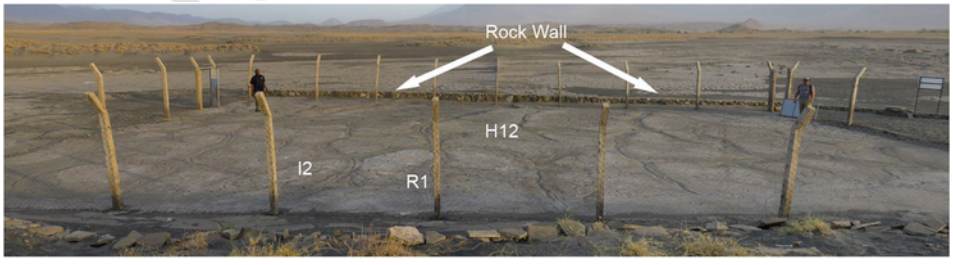

Fig. 4. The footprint site (looking south) as it appeared during the summer of 2017. The location of each footprint modeled for this study is marked by the print ID. From this view, the rock wall runs along the back of the site. Note the large desiccation cracks that cross the site. The fence and signage were installed between July 2013 and July 2015.

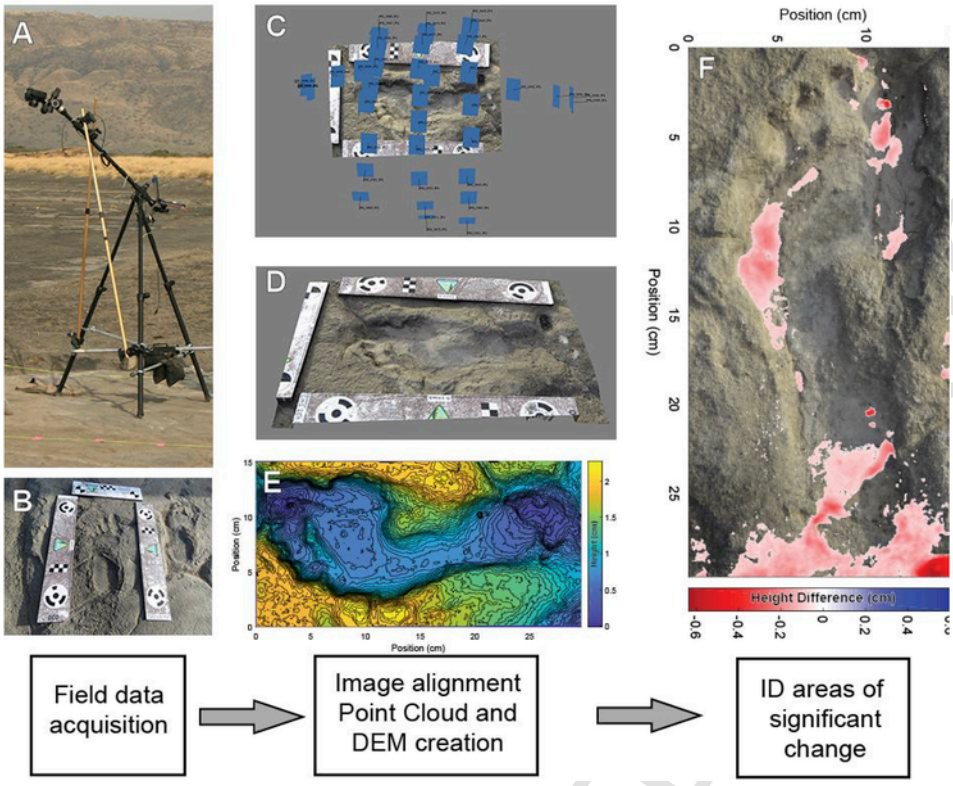

Fig. 5. Schematic of experiment workflow: (A) image capture in the field; (B) scaling using 0.01 mm calibrated scale bars with 12-bit coded markers; (C) photo alignment and cloud optimization; (D) digital model production; (E) DEM generation and contouring; (F) comparison of clouds from different years to identify areas of significant change.

Table 1
Photographic equipment and metrics used during image acquisition.

Year	Photographer(s)	Technique	Scaling axis	Equipment	Focal length	Resolution (Pixels)
2010	Metallo and Rossi	Azimuth	X-only	Canon 5D MkII; Canon EF 50 mm lens	50 mm	5616 × 3744
2012	Hatala	Azimuth	X-only	Canon 5D MkII; Canon EF 50 mm lens	50 mm	5616 × 3744
2017	Liutkus-Pierce	Obliques	X and Y	Canon Powershot SX60 HS; adjustable lens	3.8 mm	4608 × 3456

2011; Luhmann et al., 2013; James and Robson, 2014). As such, we collected converging oblique images in 2017.

4.2. Image alignment and three-dimensional model creation

Individual footprints images were aligned and transformed into a three-dimensional model using Agisoft PhotoScan Pro (www.agisoft.com) combined with the SfM point cloud workflow described by Carrivick et al., (2016) and augmented by improvements proposed by Cultural Heritage Imaging (www.culturalheritageimaging.org). For each print, between 17 and 39 pictures were used for model construction (Table 2). Generally, the more pictures used in the analysis, the higher the accuracy of a model. However, error can be introduced if multiple pictures are taken from too similar an angle or if some of the images are out of focus (Westoby et al., 2012; Mallison and Wings, 2014). Because of these issues, we excluded all imagery with an Agisoft image quality value of less than 0.5 prior to executing image alignment. Root Mean Squared (RMS) reprojection errors and were relatively consistent despite the difference in shooting equipment,

Table 2
Metadata for each of the modeled prints.

Print ID	Year	Number of Images	RMS Reprojection Error	Model Ground Resolution (mm/pix)	Scale Error (cm)	Dense Cloud Points	Mesh Faces	Mesh Vertices
R1	2010	39	0.140,265	0.0728	0.0013	4,262,457	179,999	90,489
R1	2012	26	0.156,594	0.0632	0.0246	3,489,461	199,431	100,000
R1	2017	33	0.09689	0.0792	0.0069	3,683,156	199,463	100,000
I2	2010	39	0.155,643	0.0745	0.0008	5,017,864	199,598	100,000
I2	2012	21	0.158,457	0.0654	0.0037	10,185,036	199,465	100,000
I2	2017	36	0.144,401	0.0734	0.0267	3,128,806	199,530	100,000
H12	2010	37	0.167,119	0.0841	0.0028	3,891,540	199,496	100,000
H12	2012	17	0.155,102	0.0649	0.0002	4,661,747	199,483	100,000
H12	2017	38	0.133,057	0.0776	0.0117	4,317,467	199,428	100,000

technique, and the number of images acquired (Table 2). We achieved this through the iterative removal of errant points while processing the models in Agisoft PhotoScan. Any variation in the RMS reprojection errors were likely the result of differences in the image quality and focus. Scale bar errors were <0.025 cm for making linear measurements.

4.3. Cloud alignment

By comparing point clouds generated by SfM photogrammetry from different years (i.e. differential SfM), it is possible to detect and quantify spatial changes in the relative elevations of different targets. In order to compare SfM results from two different times, each data set must be transformed into the same coordinate system. For m-to km-scale targets, GPS is often sufficient (Raber et al., 2002; Lague et al., 2013), but for smaller targets one can use local fixed control points to assist in point cloud alignments (Balaguer-Puig et al., 2017). There are many applications, however, where permanent control points are not possible due to excessive erosion, aesthetic/conservation considerations, or where the targets are too small to get meaningful geospatial resolution. At our site, installation of permanent control points was not possible, so we instead utilized a best-fitting algorithm to align the three-dimensional point clouds.

Traditional direct cloud-to-cloud comparisons using least square fits to nearest neighbor point (Girardeau-Montaut et al., 2005) or iterative closest point (ICP) (Besl and McKay, 1992) methods are useful in many applications but their use for change detection can result in large registration errors and uncertainty on targets with significant occlusion and/or on rough surfaces (Salvi et al., 2007; Bae and Lichti, 2008; Fey and Wichmann, 2017). The Multiscale Model-to-Model Cloud Compare (M3C2) algorithm developed by Lague et al., (2013) improves on these techniques by accounting for surface roughness, identifying areas of statistically significant change, and quantifying measurement uncertainty. For this reason, all change detection utilized herein was done using the M3C2 algorithm.

To align the three-dimensional data collected at different times, point clouds of each footprint were imported into CloudCompare (www.cloudcompare.org) for each year they were documented (2010, 2012, and 2017). Cropping was used to focus the alignment algorithms solely on the area of interest. In CloudCompare, each point cloud pair was coarsely aligned using a minimum of three manually-placed common points for initial registration. We chose registration points by visually analyzing the photos from each year to determine the areas that had undergone the least change and then picked common points such as unique individual clasts or junctions in desiccation cracks. By running several iterations of the coarse registration process using different manually selected points, we were able to identify accurate alignments versus ones that were errant.

During point cloud registration, it was critical to choose an appropriate overlap percentage for the data clouds that were being aligned. When using 100% overlap, the algorithm aligns the point clouds based on all points in the model. This works well when aligning unchanged surfaces. However, when change has occurred, this setting leads to an averaging of the two cloud positions and high registration errors. At lower percentages, such as 10 or 20% overlap, clouds are more susceptible to systemic problems with axial tilting and false alignments. As a result, reproducibility suffered despite the apparent decreases in error. We selected 30% overlap as it showed the best balance between returning low registration errors and having high consistency in the models produced (Supplementary Table 1; Supplementary Figures 1-2).

4.4. Change detection

To determine changes in datasets gathered at different times, we used the M3C2 algorithm (following Lague et al., 2013) on each set of prints, which allows us to quantify detectable changes from the time periods of 2010–2012, 2010–2017, and 2012–2017. The M3C2 algorithm, an analytical tool incorporated into CloudCompare, can accurately identify areas of change even when point cloud densities are inconsistent or when the surface of a cloud is noisy (Lague et al., 2013). Standard cloud-to-cloud algorithms are not able to make significant comparisons under such circumstances (Girardeau-Montaut et al., 2005). The M3C2 algorithm also considers the registration error of alignment as it determines areas where significant change (either erosion or deposition) have occurred (Fig. 6). A change is considered statistically significant if the level of detection at 95% certainty ($LOD_{95\%}$) is smaller than the measured change (Lague et al., 2013). For example, 2 ± 3 mm at a 95% confidence interval would not be considered significant, while 12 ± 3 mm would.

4.5. DEM generation and visualization

Aligned models were imported into MATLAB where all calculations and visualizations were performed using software written specifically for this study. Because model points were irregularly spaced, we produced DEMs on a regular grid (0.05 cm) using linear interpolation. Based on testing a range of grid sizes, we determined that this was a sufficiently fine grid to avoid significant aliasing of the initially aligned dense data clouds.

4.6. Method limitations and the potential for unquantifiable errors

Without permanent ground control points it is not possible to quantify the exact amount of material removed through erosion. Elevation and volumetric change estimates rely on the accuracy of the alignment of the data clouds and scaling. Based on internal checks run by Agisoft Photoscan, measurement errors along the X- and Y-axes can be computed (Table 2). However, when only one scale bar was present (2010) it is possible that there was minor distortion of measurements made along the unscaled axis. The scale bar errors returned for 2010 appear to be artificially depressed because of this accommodation. Additional scale bars were added in subsequent years in which scaling errors increased, but are more likely accurate representations of true error.

To ensure that the change detected by our method was real, all print models were run in duplicate, using subsamples of imagery from each year. These duplicate models were then compared with the originals using the M3C2 algorithm. None of the duplicate models exhibited significant derivation from the shape of the originals. While it is possible to optimize the alignment process to minimize registration errors, the resultant data clouds may not be perfectly aligned in all dimensions. Improper alignments may actually result in lower estimated errors when a surface has been eroded across its entire face or if too low of an overlap percentage is used during model alignments in CloudCompare. It is also possible, but extremely unlikely, that an entire surface could erode down uniformly. In such a scenario, the method described within this paper would identify no change when, in fact, significant change had occurred.

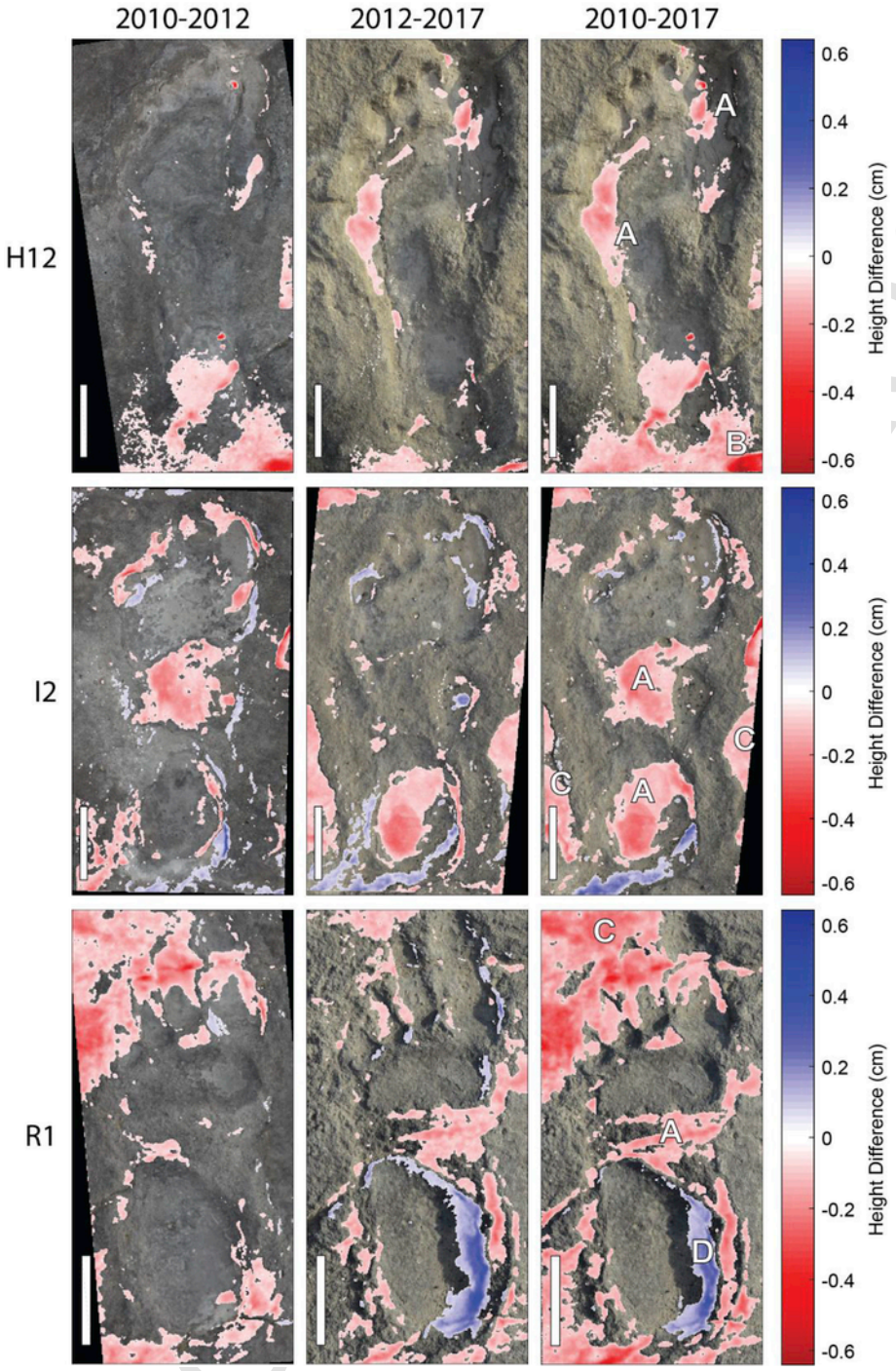

Fig. 6. Heat maps showing areas of significant change overlaid on top of footprint imagery. Red indicates negative change through time (erosion) and blue represents positive change (deposition). All images show a 0.5 × 5 cm scalebar. Areas of no change or insignificant change are transparent. Background images are from the more recent of the two compared years. Locations A-D show examples of several types of weathering. A. Abrasion. B. Boring out of a hole. C. Flaking. D. Deposition.A (For interpretation of the references to colour in this figure legend, the reader is referred to the Web version of this article.)

5. Results

5.1. Footprint H12

Footprint H12 had a maximum relief of 2.269 cm in 2010 and 2.290 cm in 2017. The lowest height values were recorded in the big toe and heel depressions with the highest heights located on the pushup levees near the fifth toe and instep (Fig. 7). The DEM resolution was fine enough to easily identify individual toe impressions, squeeze up mounds between the toes and the forefoot, detailed topography of the longitudinal arch, desiccation cracks and even small pebbles in the big toe impressions and between the arch and heel (Fig. 7c). The ability for the data to clearly show the removal of these peb-

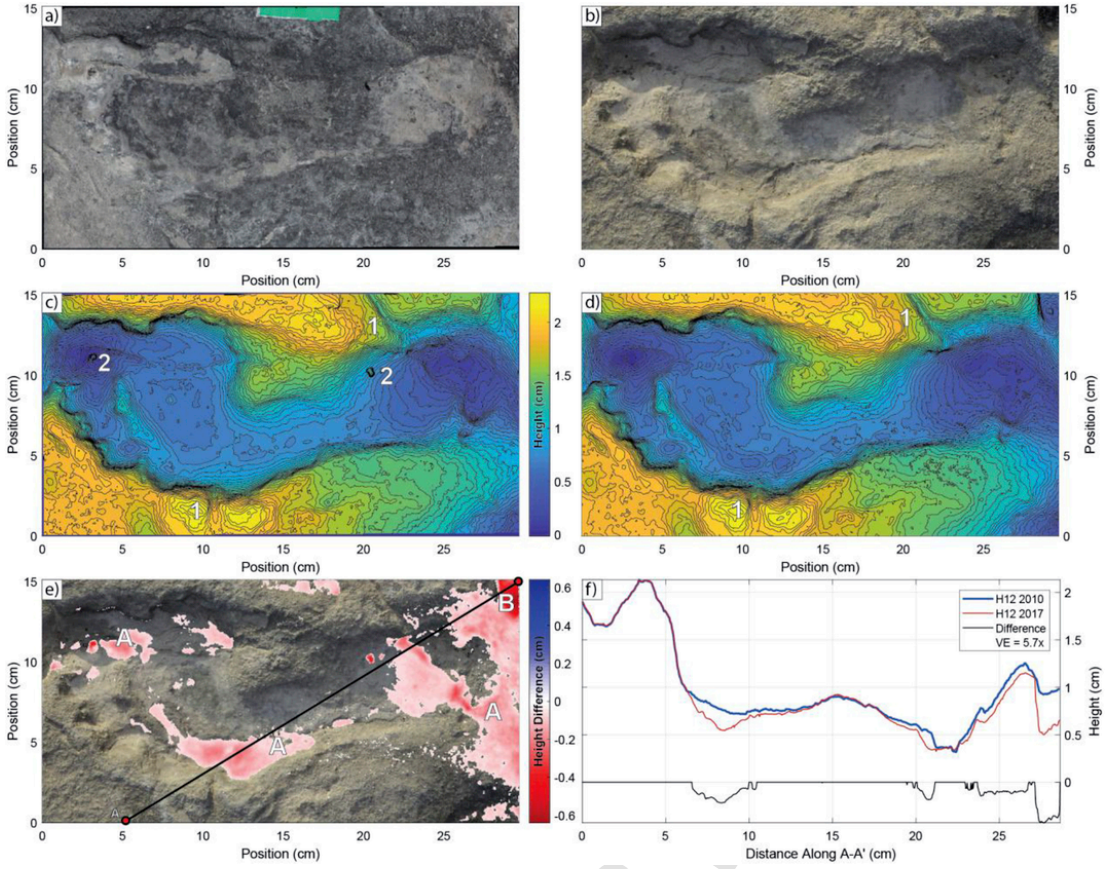

Fig. 7. Digital models of footprint H12 from 2010(a) and 2017(b). Contoured DEMs from 2010(c) and 2017(d) using a contour interval of 0.05 cm. Desiccation cracks are labeled "1", pebble locations labeled "2". (e) Difference map between the 2010 and 2017 prints. Color intensity show relative amounts of erosion (red) and deposition (blue.) Areas of abrasion are labeled "A" and boring is labeled "B". (f) Cross-sectional profile of the footprint from A to A'. All differences (black curve) are plotted as zero unless identified as significant by the M3C2 algorithm. (For interpretation of the references to colour in this figure legend, the reader is referred to the Web version of this article.)

bles indicates that the change detection methodology is successful at identifying real changes (Fig. 7d).

Though the DEMs for 2010 and 2017 are, visually, nearly indistinguishable (with the exceptions of the aforementioned pebbles), our quantitative change analyses show several areas of significant change, covering 18.33% of the total modeled surface area (Table 3). The perimeter of the print appears essentially unaltered except along the proximal heel where a modest amount of abrasion has occurred (Fig. 7). The greatest loss of material came as a hole near the heel bored down (Figs. 7 and 6A). In the boring process, loose sediment was removed from the depression through eddying within a shallow water column or wind current. Abrasion occurred within the big toe and just behind the fifth toe through the gradational removal of small amounts of material over time through primarily eolian processes.

The maximum vertical change (E_{Max}) recorded for H12 between 2010 and 2017 was 0.642 cm. Average rates of material loss (Δ_{Avg}) across the entire footprint were 0.017 cm/year or 0.119 cm over the entire seven-year period. The total volume of material removed was 9.57 cm^3, much of which was removed during the boring out of the hole by the heel (Table 3, Fig. 7f), as erosion was clearly concentrated in some areas and absent in others. Along the cross-sectional profile (A-A'), the 2010 and 2017 profiles match almost exactly from 0 to 6 cm distance and then again from 14 to 17 cm distance (Fig. 7f). This indicates that no erosion occurred at these locations and that the best-fit alignment algorithms have performed well. Where erosion

Table 3
Data related to change detection analyses run on each set of prints. Maximum vertical change between years is denoted for erosion as E_{Max} and for deposition as D_{Max}. The average change for compared prints is reported as Δ_{Avg}. Total volumetric change for each footprint is reported as Δ_{vol}.

Print ID	Years compared	Registration error	E_{Max} (cm)	D_{Max} (cm)	Δ_{Avg} (cm)	Δ_{vol} (cm^3)	Average Loss/year (cm)	Significant Change
H12	2010–2012	.000230	0.4824	0.1647	0.0915	4.7620	0.046	12.82%
H12	2012–2017	.000254	0.3577	0.1515	0.1109	2.8173	0.022	9.38%
H12	2010–2017	.000282	0.6415	0.1108	0.1192	9.5697	0.017	18.33%
I2	2010–2012	.000297	0.5755	0.4138	0.0563	4.8598	0.028	21.64%
I2	2012–2017	.000279	0.4710	0.2580	0.0556	4.6460	0.011	23.76%
I2	2010–2017	.000320	0.5989	0.4897	0.0719	9.1197	0.010	26.04%
R1	2010–2012	.000237	0.4265	0.1153	0.1149	8.6361	0.057	26.54%
R1	2012–2017	.000349	0.3908	0.4630	0.0308	2.2558	0.006	22.39%
R1	2010–2017	.000422	0.4674	0.4303	0.1222	14.5496	0.017	37.27%

did occur along the profile, the amount was highly variable, ranging from just over 0.1 cm up to nearly 0.5 cm, further indicating that the detected changes are real and not the product of misaligned meshes.

5.2. Footprint I2

Footprint I2 had a total relief of 2.021 cm in 2010 and 1.776 cm in 2017 with the lowest height values located at the back of the heel (Fig. 8). Like print H12, individual toe prints were easy to discern with a more pronounced (compared to footprint H12) squeeze-up ridge between the toes and the forefoot (Fig. 8c–d). Deposition was apparent within some of the toe depressions, but was most significant along the proximal edge of the heel (Fig. 8e). A 3 cm-diameter depression, similar to the hole discussed for H12, was located near the instep. However, unlike the hole observed in footprint H12, this depression did not erode by a detectable amount (Fig. 8c and d). As with H12, the cross sectional profile lines for I2 match almost exactly in areas in areas of no change suggesting the cloud alignment performed well (Fig. 8f).

The 2010, 2017 DEMs for I2, while exhibiting similar general patterns, showed noticeable deviation in contour patterns along the longitudinal arch and within the heel. The relief from the highest point beneath the arch to the forefoot decreased by approximately 0.25 cm over the course of the study. E_{Max} for I2 was 0.6 cm, a value very similar to that for H12. However, average the rate of loss was only 0.010 cm/year (Table 3). Significant change was detected on 26.04% of the entire modeled surface. This percentage includes both erosional change and the positive depositional change.

The boundaries between areas experiencing significant erosion and areas of no change were very sharp in I2, especially when compared with the gradational changes shown in H12 (Fig. 6). This was likely the result of substantial episodic erosion through the process of flaking as opposed to abrasion. When flaking occurs, cohesive plates of the friable sediments are removed *en masse* in response to either fluvial or eolian erosional events. Abrasion occurred along the perimeter of I2, especially along the tips of the individual toe prints but the total material removed through abrasion was less voluminous than that through flaking.

5.3. Footprint R1

Footprint R1 is a highly detailed impression that experienced the greatest change over the course of the study. R1 had a total relief of 1.974 cm in 2010 and 1.781 cm in 2017 with high points on the arch and pushup levees near the toes and low points within the heel and big toe depressions (Fig. 9). The DEMs show four of the five toes in excellent detail along with several desiccation cracks. Erosive change between the two DEMs was apparent along the arch and pushup levees surrounding the foot, while deposition was concentrated within the heel (Fig. 9e).

Over 37% of the total surface area of footprint R1 experienced significant change due to either erosion or deposition. This was, by far, the greatest area of modification among the three prints. Much of the erosion appeared to be abrasion along the periphery of the print and on topographic highs. The desiccation cracks became deeper and wider over the course of the 7 years as well. Flaking may have also

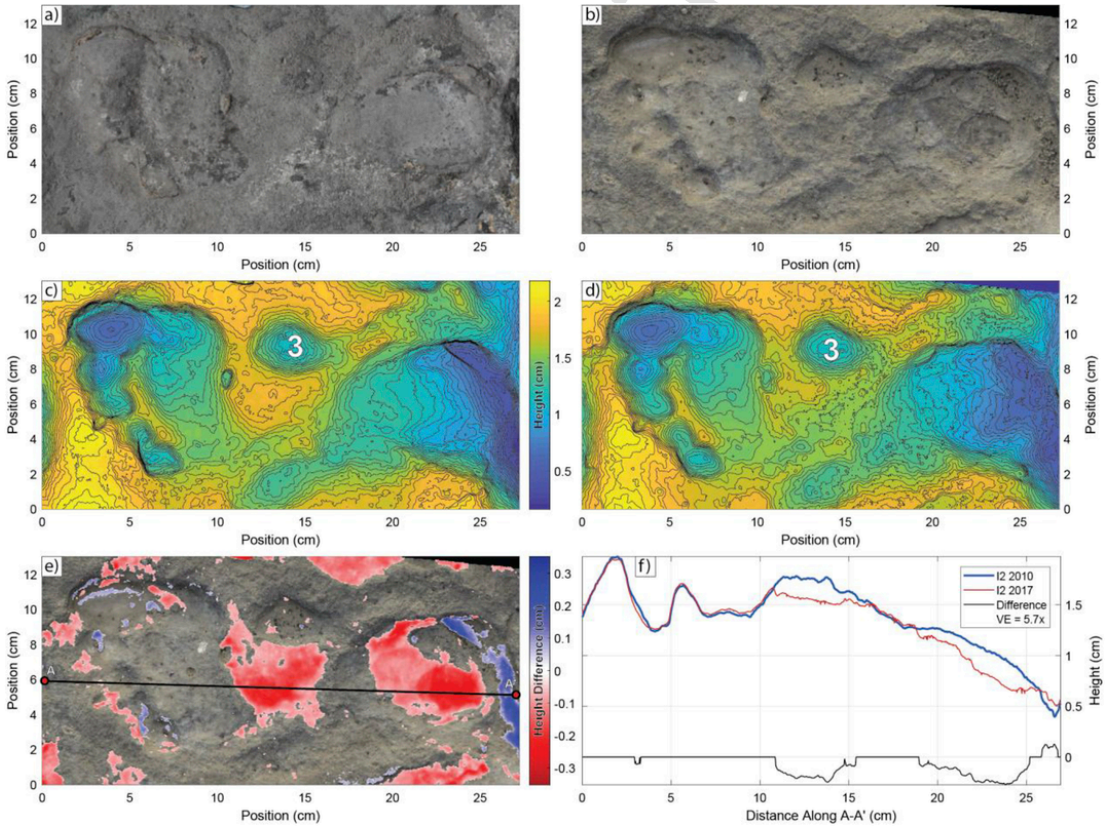

Fig. 8. Visualizations of the I2 footprint three-dimensional models from 2010(a) and 2017(b). Contoured DEMs of the I2 footprint from 2010(c) and 2017(d) using a contour interval of 0.05 cm. Depression that did not undergo significant change is labeled "3". (e) Difference map using the M3C2 algorithm between the 2010 and 2017 prints. Color intensity shows relative amounts of erosion (red) and deposition (blue.) (f) Cross-sectional profile of the footprint from A to A'. All differences (black curve) are plotted as zero unless identified as significant by the M3C2 algorithm. (For interpretation of the references to colour in this figure legend, the reader is referred to the Web version of this article.)

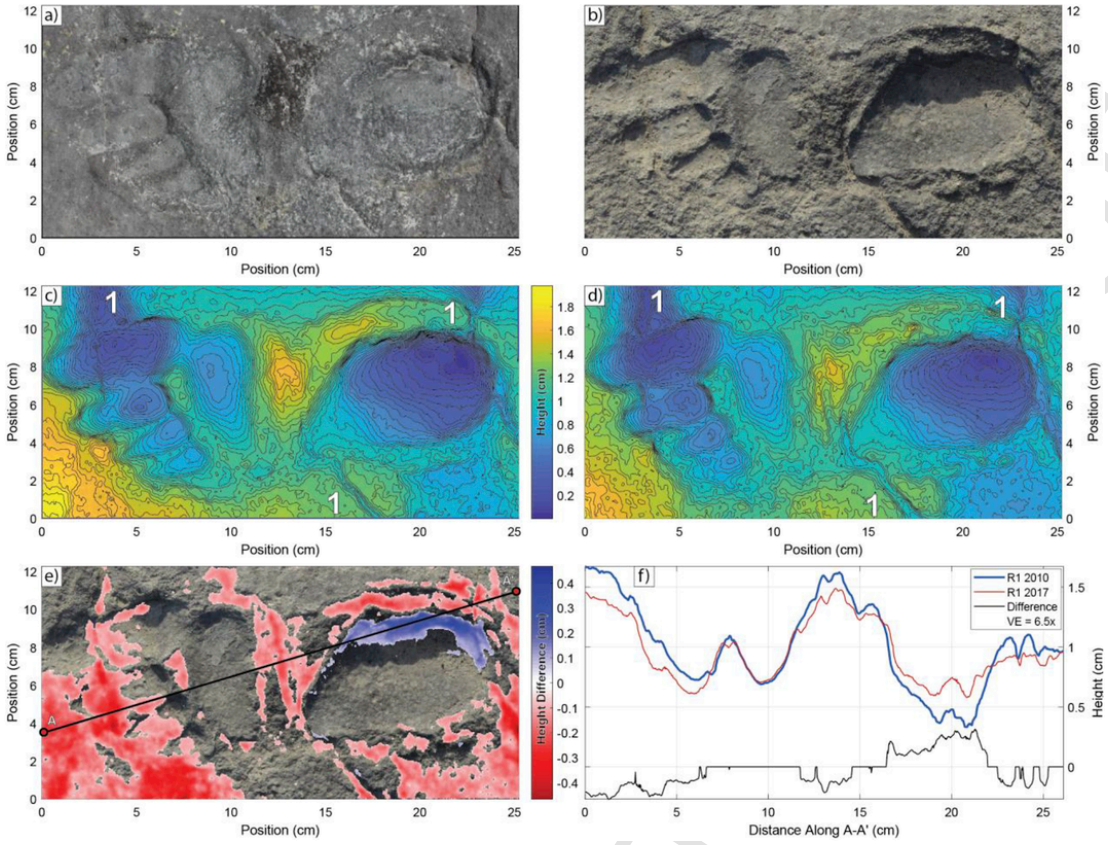

Fig. 9. Cross-section. Digital models of footprint R1 from 2010(a) and 2017(b). Contoured DEMs from 2010(c) and 2017(d) using a contour interval of 0.05 cm. Desiccation cracks are labeled "1". (e) Difference map between the 2010 and 2017 prints. Color intensity show relative amounts of erosion (red) and deposition (blue.) (f) Cross-sectional profile of the footprint from A to A'. All differences (black curve) are plotted as zero unless identified as significant by the M3C2 algorithm. (For interpretation of the references to colour in this figure legend, the reader is referred to the Web version of this article.)

occurred, resulting in the massive removal of sediments from near the toes. E_{MAX} for R1 over the entire seven-year period is 0.467 cm, less than for the other two prints. However, because R1 has a comparable Δ_{Avg} value over a much larger area of change, the total volumetric change calculated for R1 is greater than that of H12 or I2 (Table 3).

5.4. General trends

Annual erosion rates were higher from 2010 to 2012 than for 2012–2017 (Table 3). Because many of the prints were excavated for the first time during the 2010 field season it is reasonable that weathering might have been most severe initially as any poorly cemented sediments were removed quickly, leaving behind only the more indurated deposits. It is also possible that erosion events, such as floods and dust storms, may have been more severe or frequent between 2010 and 2012 than in subsequent years.

Flaking erosion was responsible for much of the material removed from the push up mounds, though it also occurred on the arch and within the heel of footprint I2 (Fig. 6). Abrasion-type erosion was most common right along the rims of the impressions, along the arches, and in isolated small patches on the squeeze-ups mounds. Where the flaking boundaries were stark, the abrasion-type erosion boundaries appeared more diffuse. Flaking resulted in changes of about 0.20 cm (Fig. 8f) while areas subjected to abrasion-style erosion appear to lose 0.15 cm or less material. Boring resulted in the most severe loss of material (>0.4 cm) (Fig. 7f).

Deposition occurred primarily in the heel depressions of the prints and was in the form of loose, windblown sediments. Depositional change does not represent any permanent change to the print, just the temporary accumulation of wind-blown debris. Careful cleaning of each print prior to imaging would likely have removed most, if not all, depositional returns.

6. Discussion

For some of the footprints at Engare Sero, qualitative observations of erosion can be made by visual inspection and comparison of photographs from different years. For example, visual comparison of footprint I2 between 2010 and 2017 identifies several areas of suspected erosion and deposition (Fig. 8). The arch in Fig. 8b has clearly been modified and the removal of a modest disc of sediment is apparent within the heel. While visible inspection can be helpful for qualitative evaluations of erosion, changes in the lighting or the quality of imagery can lead to failing to identify areas of significant erosion or suspecting erosion where the print has actually been stable. For example, by looking at the same two images of I2, one might suspect the depression near the arch increased dramatically from 2010 to 2017 when in reality, the change was not significant. By using SfM photogrammetry, we can quantitatively determine locations and magnitudes of change over time.

Considering the overall relief of all of the prints is approximately 2 cm, one might infer that at the current average rates of erosion (0.010–0.017 cm/yr), the prints might last a few decades before being

lost. However, fidelity of the prints is already noticeably decreased as the arches have been worn down, decreasing internal relief, especially on prints I2 and R1 (Figs. 8 and 9). Anecdotal evidence supports our finding that the prints are eroding away at observable rates. The prints selected for this study were some of the most well-formed and obvious. Many other prints had much lower relief and will likely disappear more quickly. In 2017, we were unable to locate several of the fainter prints that were identifiable in 2010.

Though we have calculated Δavg rates for each print, it is unlikely that erosion rates are consistent over time. It is more likely that long periods of stasis were interrupted by punctuated erosional episodes. Based on the friable nature of the substrate and its tendency to flake, it is reasonable to suspect much of the material was/will be removed *en masse* as opposed to incrementally. Two lines of evidence support this hypothesis: 1) the flaking-type erosion (Fig. 6) has very sharp boundaries as opposed to the more gradational margins of areas denoted as abrasion-type erosion, suggesting that the flaking occurred *en masse* while the abrasion was more smooth and incremental and, 2) the striking similarities seen in the topographic profiles of the different footprints in areas where "insignificant change" was reported (Figs. 7f, 8f and 9f). Erosional rates may have been reduced by the construction of a rock wall that was installed sometime between July 2013 and July 2015, along the southern and western borders of the footprint site to divert seasonal flood waters away from the footprints. Flooding has the highest potential for severely altering the footprint site and from 2010 to 2012, it is possible that the site experienced more frequent or stronger flooding events than from 2012 until the wall was built sometime before July 2015. This would account for the higher annual loss that all three prints experienced between 2010 and 2012 (Table 3). If additional imagery is collected from the same footprints in two to three years, we may then be able to better constrain the effect the wall has had on rates of erosion.

The total area that we could detect as modified by erosion varied appreciably over the seven years from print to print with H12 experiencing erosion over the smallest portion of its exposed surface (18.33%) and R1 experiencing the most (37.27%) (Table 3). Because these percentages only include areas of statistically significant change, as reported by the M3C2 differencing algorithm, the area estimates should be considered minimums. It is reasonable to suspect that most of trampled surface experienced some erosion or deposition, but that the changes were below our detection limit given our source photos and methods. Histograms reporting the number of mesh vertices at various depositional/erosional ranges for each of the modeled prints show that the most common changes were near the limit of detection calculated by the M3C2 algorithm for our data (Fig. 10). It should be noted that these histograms indicate only the number of vertices and are not appropriate for making quantitative measurements of area or volume as spacing between vertices is non-uniform. Nonetheless, the presence of modal values near the detection limits suggests that the footprints have likely experienced additional erosion/deposition beyond what we can reliably detect with our current data. Over a longer time interval, the changes will be larger and possibly detectable; however, more change does not necessarily mean that the change would be easier to quantify. In heavily altered prints, the lack of a sufficient percentage of overlapping points would decrease the accuracy in cloud-to-cloud alignments and could potentially produce unreliable results. In cases where large amounts of erosion require monitoring with SfM methods, the installation of permanent ground control points would likely be necessary.

The accuracy and precision of change detection described could be limited by the number and quality of images used to create the 3D models as well as the initial manual alignment of the meshes. To ensure that the areas of detected erosion are real and not simply artifacts of the source images, we created several sets of duplicate models of each track in this study using a random subset of the original imagery. The duplicate models were then aligned with the original models at 100% overlap. Change detection comparisons of these duplicate models identified no areas of significant change between models. Additionally, change detection comparisons between the duplicate 2017 and original 2010 models produced nearly identical results to the models using the full image suite (Supplementary Figure 3). Any minor deviations in the duplicate runs are likely the result of slight dif-

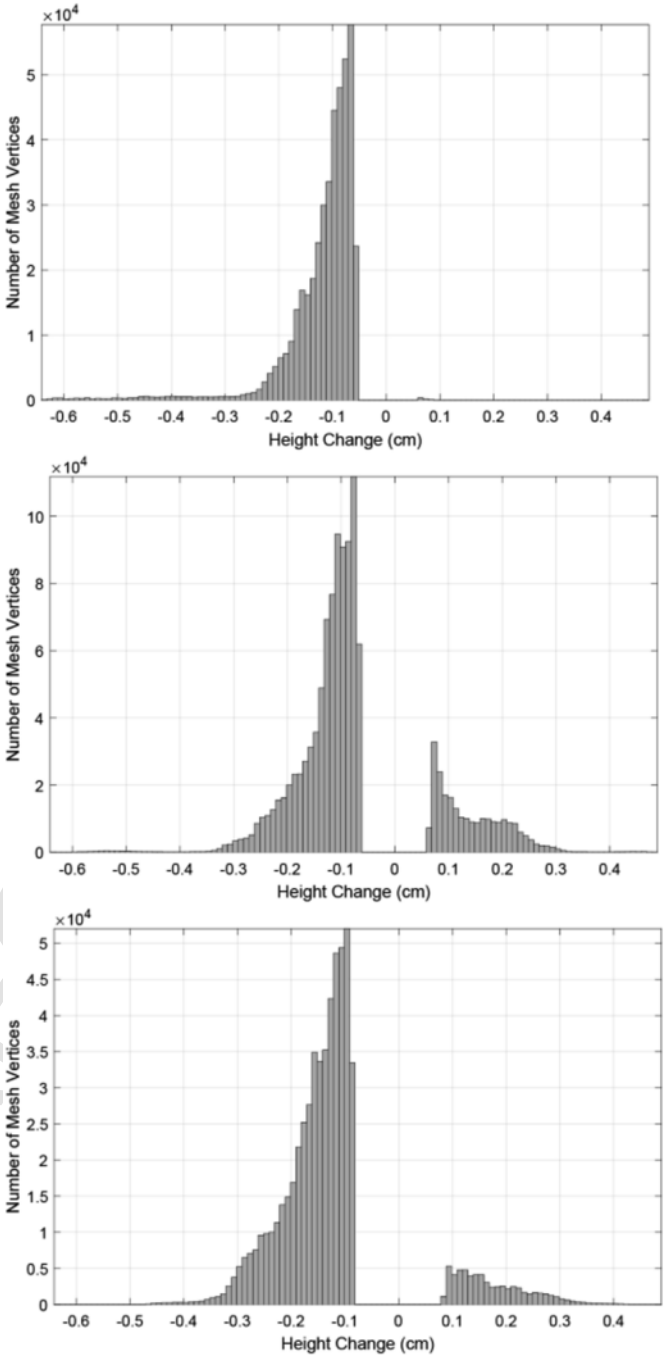

Fig. 10. Histograms of height changes from each of the three prints: a) H12, b) I2, and c) R1. For each footprint the detection limit was approximately ±0.1 cm, which also corresponds to nearly modal values of change.

ferences in the initial manual alignment of the meshes, but the overall locations and magnitudes of detected changes presented here are therefore real and not artifacts.

6.1. Causes of erosion

The loss of relief observed in the analyzed footprints comes from both chemical and physical erosion processes. Physical erosion due to flooding of the Engare Sero river is a primary concern as the site has been inundated repeatedly in response to intense rainfall events, especially during the rains of Masika (March–May) and Mvuli (November-mid January). Under arid conditions that are common in the dry season in northern Tanzania (May–October), desiccation of entrained clays and abrasion from windblown sand both work to break down exposed deposits. There are small channels and desiccation fractures crossing the site that likely experienced enhanced rates of erosion due to channelized flow of runoff (Fig. 2).

Human and animal activity may have also played a role in site deterioration since excavation. Prior to the construction of the rock wall, there was no impediment to keep vehicles from driving across the footprint site or to keep zebra and wildebeest herds off the surface. A small wall and fence now surround the footprint site, keeping vehicles and foraging animals away (Fig. 4). Unfortunately, when tourists visit the footprint site, there is no physical barrier to prevent individuals from walking on and potentially damaging the footprints as the gate on the fence is currently not functional. A common practice when tourists visit footprint sites is to measure one's own footprint by placing it within one of the preserved prints, potentially damaging it.

Chemical processes also likely played a role in both the preservation and degradation of the footprints at the Engare Sero site. The footprints were initially pressed into soft volcaniclastic sediments found along the southern shoreline of paleo-Lake Natron. A low-energy lahar covered the prints shortly after deposition (Liutkus-Pierce et al., 2016). The now-exposed layer is more durable than the original sediments due to cementation by calcite and magadiite that was likely precipitated from wetting of the buried deposit by alkaline ground- or surface-water. Burial was critical for preservation, as Liutkus-Pierce et al., (2016) showed that newly cemented ash of phonolitic composition was easily remobilized when inundated by various alkaline solutions at surface conditions. While the newly exposed footprinted surface at Engare Sero appears to be more indurated and resistant to sediment remobilization than the fresh ash of Liutkus-Pierce et al., (2016) experiment, repetitive wetting and drying is likely destabilizing the material's integrity now that it has been excavated. While we do not have water chemistry data from these flooding events, groundwater that flows through the area and emerges as springs often has a high alkalinity (35–56 meq/L) and total dissolved solids (TDS) (5000–10,000 $\mu S\,cm^{-1}$) (Deocampo, 2002). Thus, it is likely that surface water flowing through similar deposits would absorb proportional levels of dissolved ions. While the initial cementation is responsible for the strength of the deposit, repeated precipitation of secondary minerals may produce a wedging effect and weaken the foot-printed sediments, as crystals grow within tiny cracks already present in the ash layers and force those cracks to expand.

6.2. Potential effects on anthropological inferences

Aside from the effects on long-term site preservation, erosion has the potential to influence the anthropological inferences that can be garnered from hominin footprints. The entire erosional history of a footprint site is likely to be largely unknown; for example, episodic erosion could have occurred for centuries before the first prints were identified at Engare Sero in 2006. However, by studying erosional processes that begin to occur once a site is excavated, this study and others (e.g., Wiseman and De Groote, 2018) are just beginning to shed light on how and to what extent these processes may introduce previously unaccounted-for error to inferences drawn from the morphology of ancient human footprints. For example, Wiseman and De Groote (2018) found that, after initial excavation, tidal action significantly altered both the outline metrics (length and width) and the internal topography of human footprints at Formby Point, a Holocene site in the UK. These outline metrics are regularly used by paleoanthropologists to estimate body size, while the internal topography is often the diagnostic tool through which foot and lower limb kinematics are inferred. The erosion of the Formby Point footprints was rapid and severe– footprint-bearing sediments were completely obliterated after just two weeks of exposure to tidal erosion (Wiseman and De Groote, 2018). In the case of Engare Sero, the rate and magnitude of erosion were far less; however, seven years of more subtle erosion may still have noticeable effects on footprint parameters that influence anthropological inferences.

Across the three Engare Sero footprints analyzed here, one of the general footprint features most affected by erosion since 2010 is the outer rim (e.g., Fig. 9e). Even a cursory visual inspection of footprint images and DEMs reveals that the perimeter of these prints has been blurred over the past seven years (e.g., Fig. 9a–d). The outline size of the footprint has slightly expanded, which would cause body size estimates to slightly increase. Further, more poorly defined footprint borders hint at a likely decline in repeatability of outline size measurements. Apart from these effects on footprint size, we observed perhaps more concerning effects of erosion on the footprints' internal topographies. Each footprint examined here experienced a maximum vertical erosion of approximately 0.5 cm (Table 3), and this magnitude was not uniform but instead varied laterally across regions (Fig. 6). Ever since some of the earliest functional studies of hominin footprints (e.g**.,** Day and Wickens, 1980), their internal topography has been assumed to represent in some way a combination of plantar foot anatomy and foot motion. If there are spatial differences in how a footprint's internal topography is affected by erosion, then this may lead to different anatomical or functional interpretations, depending on how long footprints have been exposed. For example, a researcher who arrived at Engare Sero in 2017 to study these footprints might infer that whoever created them had a (larger) lower-arched foot, and perhaps used a different pattern of foot motion than was inferred by another researcher who studied the very same prints in 2010. Fractions of centimeters of erosion may affect body size estimates only marginally, when considering errors already inherent to those predictions (e.g., prediction intervals for regression), but effects on qualitative interpretations based on the internal topographies of footprints that are just a few centimeters deep may be more significant. Ultimately, these results highlight a potentially poorly-understood and previously unquantified effect of erosion on the degradation of footprint morphology, in which more research can advance our understandings of how (and how quickly) footprints can physically change over time and how we may need to adapt best practices for footprint excavations.

7. Conclusions

In this paper, we describe and quantify the erosional degradation of individual human footprints from the Engare Sero footprint site using SfM photogrammetry in the absence of permanent ground control points. We show that, when paired with a rigorous workflow, low

cost SfM data collected at different times can be used to quantify complex spatially-variable rates of erosion/deposition of exposed hominid footprints. Our analyses show that the prints at Engare Sero experienced average rates of erosion over the seven years of the study ranging from 0.10 to 0.17 mm/year with areas of higher topography and steeper slopes, like arches, pushup mounds, and squeeze-up ridges between toes experiencing erosion at higher rates. Erosion presented in three basic forms; flaking, boring, and abrasion.

Erosion at the Engare Sero site appears to be episodic with punctuated moments of larger loss interspersed amid periods of relative stability. With each year that elapses, the quality of the footprint site decreases. This has an impact on the viability and longevity of the site as a potential tourist attraction as well as a detrimental effect on the suitability of the site to produce robust data for future scientific inquiries, especially studies that rely on morphometric measurements. The addition of the rock wall to divert floodwaters around the site may be a positive first step towards preservation of the site. We identified that erosion was, in general, more severe prior to the installation of the rock wall, but because we do not have a dataset that completely postdates the installation of the wall, we cannot confidently conclude that the wall has been successful at reducing erosion at the site.

While it is impossible to physically preserve every site, this paper provides a quantitative and low-cost methodology that can be used by researchers and conservation groups to not only digitally preserve footprint sites but also to monitor short- and long-term erosional change and make more informed decisions about the sustainability of footprint sites for both tourism and research purposes.

Data availability

Three-dimensional models of several of the prints in this study are available through the Smithsonian Institution Digitization Program Office. https://play.autodesk.com/pub/si-si-default-v4?cid=4006329.

Acknowledgements

The authors wish to acknowledge funding received from the National Geographic Society's Committee for Research and Exploration (8748-10), the National Science Foundation (NSF BCS-1128170), the Leakey Foundation (71483-0001), the Explorers Club, Appalachian State University (the University Research Council and the Office of International Development and Research), and the Smithsonian Institution's Human Origins Program and Digitization Program Office. In addition, we thank colleagues who assisted in field and laboratory efforts; Anthony Love, Sara Mana, Al Deino, Sarah Carmichael, Guichuon Hou, Seth Hewitt, Briana Pobiner, Will Harcourt-Smith, Brian Richmond, Katelyn McGinnis, Katie Wolf, Benedict Pius, and Kongo Sakkae. Tim Leach, Godfrey Ollemoita, Marc Basseporte, and Ndashy Munuo (Good Earth Tours) provided logistical support and we thank the Tanzania Department of Antiquities and the Commission on Science and Technology (COSTECH) for their continued cooperating and permission to work at Engare Sero. Kathy Adams and Max Anderson supported the development of the online model content. We give our most sincere thanks to our Project Director, Jim Brett. Finally, the manuscript benefitted greatly from constructive reviews by Neil Roach, Matteo Belvedere, and a third, anonymous reviewer.

Appendix A. Supplementary data

Supplementary data related to this article can be found at https://doi.org/10.1016/j.quascirev.2018.07.006.

References

Adams, T.L., Strganac, C., Polcyn, M.J., Jacobs, L.L., 2010. High resolution three-dimensional laser scanning of the type specimen of eubrontes (?) glenrosensis shuler, 1935, from the comanchean (lower cretaceous) of Texas: implications for digital archiving and preservation. Palaeontol. Electron. 13 (3), 1T:11p.

.

Altamura, F., Bennett, M.R., D'Août, K., Gaudzinski-Windheuser, S., Melis, R.T., Reynolds, S.C., Mussi, M., 2016. Archaeology and ichnology at Gombore II-2, Melka Kunture, Ethiopia: everyday life of a mixed-age hominin group 700,000 years ago. Sci. Rep. 8, 2815.

Ashley, G.M., Liutkus, C.M., 2002. Tracks, trails, and trampling by large vertebrates in a rift valley paleo-wetland, lowermost Bed II, Olduvai Gorge, Tanzania. Ichnos 9, 23–32.

Ashton, N., Lewis, S.G., De Groote, I., Duffy, S.R., Bates, M., Bates, R., Hoare, P., Lewis, M., Parfitt, S.A., Peglar, S., Williams, S., Williams, C., Stringer, C., 2014. Hominin footprints from early Pleistocene deposits at Happisburgh, UK. PLoS One 9 (2), e88329.

Bae, K.-H., Lichti, D.D., 2008. A method for automated registration of unorganized point clouds. ISPRS J. Photogrammetry Remote Sens. 63, 36–54.

Balaguer-Puig, M., Marques-Mateu, A., Lerma, J., Ibanez-Asensio, S., 2017. Estimations of small-scale soil erosion in laboratory experiments with structure from motion photogrammetry. Geomorphology 295, 285–296.

Behrensmeyer, A., Laporte, L., 1981. Footprints of a Pleistocene hominid in northern Kenya. Nature 289, 167–169.

Belvedere, M., Bennett, M.R., Marty, D., Budka, M., Reynolds, S.C., Bakirov, R., 2018. Stat-tracks and mediotypes: powerful tools for modern ichnology based on 3D models. Peer J. 6, https://doi.org/10.7717/peerj.4247, e4247.

Bemis, S.p., Micklethwaite, S., Turner, D., James, M.R., Akciz, S., Thiele, S.T., Ali Bangash, H., 2014. Ground-based and UAV-Based photogrammetry: a multi-scale, high-resolution mapping tool for structural geology and paleoseismology. J. Struct. Geol. 69, P163–P178. https://doi.org/10.1016/j.jsg.2014.10.007.

Bennett, M.R., Harris, J.W., Richmond, B.G., Braun, D.R., Mbua, E., Kiura, P., Olago, D., Kibunjia, M., Omuombo, C., Behrensmeyer, A.K., Huddart, D., Gonzalez, S., 2009. Early Hominin foot morphology based on 1.5-million-year-old footprints from Ileret, Kenya. Science 323, 1197–1201. https://doi.org/10.1126/science.1168132.

Bennett, M.R., Falkingham, P., Morse, S.A., Bates, K., Crompton, R.H., 2013. Preserving the impossible: conservation of soft-sediment hominin footprint sites and strategies for three-dimensional digital data capture. PLoS One 8, e60755.

Bennett, M.R., Reynolds, S.C., Morse, S.A., Budka, M., 2016. Laetoli's lost tracks: 3D generated mean shape and missing footprints. Nat. Sci. Rep. 6, 21916.

Berge, C., Penin, X., Pellé, , 2006. New interpretation of Laetoli footprints using an experimental approach and Procrustes analysis: preliminary results. Comptes Rendus Palevol 5, 561–569.

Besl, P.J., McKay, N.D., 1992. A method for registration of 3-D shapes. IEEE Trans. Pattern Anal. Mach. Intell. 14, 239–256.

Bosworth, W., 1987. Off-axis volcanism in the Gregory rift, east Africa: implications for models of continental rifting. Geology 15, 397–400 https://doi.org/10.1130/0091-7613.

Bustos, D., Jakeway, J., Urban, T.M., Holliday, V.T., Fenerty, B., Raichlen, D.A., Budka, M., Reynolds, S.C., Allen, B.D., Love, D.W., Santucci, V.L., Odess, D., Willey, P., McDonald, H.G., Bennett, M.R., 2018. Footprints preserve terminal Pleistocene hunt? Human-sloth interactions in North America. Sci. Adv. 4, eaar7621.

Carrivick, J.L., Smith, M.W., Quincey, D.J., 2016. Structure from Motion in TheGeosciences. Wiley- Blackwell, Chichester, UK https://doi.org/10.1002/9781118895818.

Charteris, J., Wall, J.C., Nottrodt, J.W., 1981. Functional reconstruction of gait from the Pliocene hominid footprints at Laetoli, northern Tanzania. Nature 290, 496–498.

Charteris, J., Wall, J.C., Nottrodt, J.W., 1982. Pliocene hominid gait: new interpretations based on available footprint data from Laetoli. Am. J. Phys. Anthropol. 58, 133–144.

Citton, P., Nicosia, U., Nicolosi, I., Carluccio, R., Romano, M., 2015. Elongated theropod tracks from the cretaceous apenninic carbonate platform of southern latium (central Italy). Palaeontol. Electron. 18, 1–12.

Citton, P., Romano, M., Salvador, I., Avanzini, M., 2017. Reviewing the upper Pleistocene human footprints from the 'Sala dei Misteri' in the Grotta della Basura (Toirano, northern Italy) cave: an integrated morphometric and Morpho-classifica-

tory approach. Quat. Sci. Rev. 169, 50–64. https://doi.org/10.1016/j.quascirev.2017.05.016.
Crompton, R.H., Pataky, T.C., Savage, R., D'Août, K., Bennett, M.R., Day, M.H., Bates, K., Morse, S., Sellers, W.I., 2012. Human-like external function of the foot, and fully upright gait, confirmed in the 3.66 million year old Laetoli hominin footprints by topographic statistics, experimental footprint-formation and computer simulation. J. R. Soc. Interface 9, 707–719.
Dalton, R., 2008. Fears for oldest human footprints. Nature 451, 118. https://doi.org/10.1038/451118a.
Dawson, J.B., 1962. The geology of Oldoinyo lengai. Bull. Volcanol. 24, 349–387.
Dawson, J.B., 1992. Neogene tectonics and volcanicity in the North Tanzania sector of the Gregory Rift Valley: contrasts with the Kenya sector. Tectonophysics 204, 81–92. https://doi.org/10.1016/0040-1951(92)90271-7.
Dawson, J.B., 2008. The Gregory Rift Valley and Neogene-Recent Volcanoes of Northern Tanzania: Geological Society Memoir No. 33. The Geological Society, London.
Dawson, J.B., Powell, D.G., 1969. The Natron-Engaruka explosion crater area, northern Tanzania. Bull. Volcanol. 33, 761–817.
Day, M.H., Wickens, E.H., 1980. Laetoli Pliocene hominid footprints and bipedalism. Nature 286, 385–387.
Demas, M., Agnew, N., 2006. Decision making for conservation of archaeological sites: the example of the Laetoli hominid trackway, Tanzania. In: Of the Past, for the Future, Integrating Archaeology and Conservation Getty Conservation Institute Symposium Proceeding Publication of the 5th World Archaeological Congress. pp. 64–72.
Deocampo, D.M., 2002. Sedimentary processes and lithofacies in lake-margin groundwater-fed wetlands in East Africa. In: In: Ashley and, Renaut (Ed.), Sedimentation in Continental Rifts, vol. 73, SEPM special publication, pp. 295–308.
Falkingham, P.L., 2012. Acquisition of high resolution three-dimensional models using free, open- source, photogrammetric software. Palaeontol. Electron. 15, 1.1.T.
Falkingham, P.L., 2014. Interpreting ecology and behaviours from the vertebrate fossil track record. J. Zool. 292, 222–228.
Falkingham, P.L., Bates, Karl T., Avanzini, Marco, Bennett, Matthew, Bordy, Emese M., Breithaupt, Brent H., Castanera, Diego, Citton, Paolo, Díaz-Martínez, Ignacio, Farlow, Jim O., Fiorillo, hony R., Gatesy, Stephen M., Getty, Patrick, Hatala, Kevin G., Hornung, Jahn J., Hyatt, James A., Klein, Hendrik, Lallensack, Jens N., Martin, Anthony J., Marty, Daniel, Matthews, Neffra A., Meyer, Christian A., Milàn, Jesper, Minter, Nicholas J., Razzolini, Novella L., Romilio, Anthony, Salisbury, Steven W., Sciscio, Lara, Tanaka, Ikuko, Wiseman, Ashleigh L.A., Xing, L.D., Belvedere, Matteo, 2018. A standard protocol for documenting modern and fossil ichnological data. Palaeontology
Fey, C., Wichmann, V., 2017. Long-range terrestrial laser scanning for geomorphological change detection in alpine terrain – handling uncertainties. Earth Surf. Process. Landforms 42, 789–802. https://doi.org/10.1002/esp.4022.
Girardeau-Montaut, D., Roux, M., Marc, R., Thibault, G., 2005. Change detection on point cloud data acquired with a ground laser scanner. Int. Arch. Photogram. Rem. Sens. Spatial Inf. Sci. 36 (Part 3), 30–35.
Gonzalez, S., Huddart, D., Bennett, M.R., Gonzalez-Huesca, A., 2006. Human footprints in Central Mexico older than 40,000 years. Quat. Sci. Rev. 25, 201–222. https://doi.org/10.1016/j.quascirev.2005.10.004.
Hatala, K.G., Demes, B., Richmond, B.G., 2016a. Laetoli footprints reveal bipedal gait biomechanics different from those of modern humans and chimpanzees. Proc. R. Soc. B 283, 20160235.
Hatala, K.G., Roach, N.T., Ostrofsky, K.R., Wunderlich, R.E., Dingwall, H.L., Villmoare, B.A., Green, D.J., Harris, J.W.K., Braun, D.R., Richmond, B.G., 2016b. Footprints reveal direct evidence of group behavior and locomotion in Homo erectus. Sci. Rep. 6, 28766.
Helm, C.W., McCrea, R.T., Cawthra, H.C., Lockley, M.G., Cowling, R.M., Marean, C.W., Thesen, G.H., Pigeon, T.S., Hattingh, S., 2018. A new Pleistocene hominin tracksite from the Cape south Coast, South Africa. Sci. Rep. 8, 3772. https://doi.org/10.1038/s41598-018-22059-5.
James, M.R., Robson, S., 2014. Mitigating systematic error in topographic models derived from UAV and ground-based image networks. Earth Surf. Process. Landforms 39, 1413–1420 https://doi.org/10.1002/esp.3609.
James, M.R., Robson, S., Smith, M.W., 2017. 3-D uncertainty-based topographic change detection with structure-from-motion photogrammetry: precision maps for ground control and directly georeferenced surveys. Earth Surf. Process. Landforms 42, 1769–1788. https://doi.org/10.1002/esp.4125.
Javernick, L., Brasington, J., Caruso, B., 2014. Modeling the topography of shallow braided rivers using Structure-from-Motion photogrammetry. Geomorphology 213, 166–182. https://doi.org/10.1016/j.geomorph.2014.01.006.
Johannesson, T., Bjornsson, H., Magnusson, E., Gudmundsson, S., Palsson, F., Sigurdsson, O., Thorsteinsson, T., Berthier, E., 2013. Ice-volume changes, bias estimation of mass-balance measurements and changes in subglacial lakes derived by lidar mapping of the surface Icelandic glaciers. Ann. Glaciol. 54 (63), 63–74.
Johnson, K., Nissen, E., Saripalli, S., Arrowsmith, J.R., McGarey, P., Scharer, K., Williams, P., Blisniuk, K., 2014. Rapid mapping of ultrafine fault zone topography with structure from motion. Geosphere 10, 969–986. https://doi.org/10.1130/GES01017.1.
Kobler, A., Pfeifer, N., Ogrinc, P., Todorovski, L., Oštir, K., Džeroski, S., 2007. Repetitive interpolation: a robust algorithm for DTM generation from aerial laser scanner data in forested terrain. Rem. Sens. Environ. 108, 9–23. https://doi.org/10.1016/j.rse.2006.10.013.
Lague, D., Brodu, N., Leroux, J., 2013. Accurate 3D comparison of complex topography with terrestrial laser scanner: applicationto the Rangitikei canyon (N-Z). ISPRS J. Photogrammetry Remote Sens. 82, 10–26. https://doi.org/10.1016/j.isprsjprs.2013.04.009.
Leakey, M.D., 1981. Tracks and tools. Phil. Trans. Roy. Soc. B 292, 95–102.
Leakey, M.D., Hay, R.L., 1979. Pliocene footprints in the Laetolil beds at Laetoli, northern Tanzania. Nature 22, 317–323.
Liutkus-Pierce, C.M., Zimmer, B.W., Carmichael, S.K., McIntosh, W., Deino, A., Hewitt, S.M., McGinnis, K.J., Hartney, T., Brett, J., Mana, S., Deocampo, D., Richmond, B.G., Hatala, K., Harcourt-Smith, W., Pobiner, B., Metallo, A., Rossi, V., 2016. Radioisotopic age, formation and preservation of Late Pleistocene human footprints at Engare Sero, Tanzania. Palaeogeogr. Palaeoclimatol. Palaeoecol. 463, 68–82. https://doi.org/10.1016/j.palaeo.2016.09.019.
Lofgren, D.L., Greening, J.A., Johnson, C.F., Lewis, S.J., Torres, M.A., 2006. Fossil tracks at the Raymond Alf Museum of Paleontology and management of tracks on public lands. Bull. N. M.Mus. Nat. Hist. Sci. 34, 109–118.
Lucieer, A., deJong, S.M., Turner, D., 2013. Mapping landslide displacements using structure from motion (SfM) and image correlation of multi-temporal UAV photography. Prog. Phys. Geogr. 38 (1), 97–116. https://doi.org/10.1177/0309133313515293.
Luhmann, T., Robson, S., Kyle, S., Boehm, J., 2013. Close-range Photogrammetry and 3D Imaging, second ed. Walter de Gruyter, Berlin/Boston https://doi.org/10.1515/9783110302783.
Mallison, H., Wings, O., 2014. Photogrammetry in paleontology – a practical guide. J. Paleontol. Technol. 12, 1–31.
Marteau, B., Vericat, D., Gibbins, C., Batalls, R.J., Green, D.R., 2017. Application of Structure-From- Motion photogrammetry to river restoration. Earth Surf. Process. Landforms 42, 503–515. https://doi.org/10.1002/esp.4086.
Marty, D., Strasser, A., Meyer, C.A., 2009. Formation and taphonomy of human footprints in microbial mats of present-day tidal-fl at environments: implications for the study of fossil footprints. Ichnos 16, 127–142.
Marty, D., Belvedere, M., Razzolini, N.L., Lockley, M.G., Paratte, G., Cattin, M., Lovis, C., Meyer, C.A., 2017. The tracks of giant theropods (Jurabrontes curtedulensis ichnogen & ichnosp. nov.) from the Late Jurassic of NW Switzerland: palaeoecological & palaeogeographical implications. Hist. Biol. 1–29. https://doi.org/10.1080/08912963.2017.1324438.
Masao, F.T., Ichumbaki, E.B., Cherin, M., Barili, A., Boschian, G., Iurino, D.A., Menconero, S., Moggi- Cecchi, J., Manzi, G., 2016. New footprints from Laetoli (Tanzania) provide evidence for marked body size variation in early hominins. eLife 5, e19568.
Matthews, N.A., 2008. Resource Documentation, Preservation, and Interpretation: Aerial and Close- Range Photogrammetric Technology in the Bureau of Land Management. U.S. Department of the Interior, Bureau of Land Management. National Operations Center, Denver, Colorado.
Matthews, N.A., Noble, T.A., Breithaupt, B.H., 2006. The application of photogrammetry, remote sensing and geographic information systems (GIS) to fossil resource management. Bull. N. M.Mus. Nat. Hist. Sci. 34, 119–131.
Matthews, N., Noble, T., Breithaupt, B., 2016. Close-range photogrammetry for 3-d ichnology: the basics of photogrammetric ichnology. In: Falkingham, P., Marty, D., Richter, A. (Eds.), Dinosaur Tracks: the Next Steps. Indiana University Press, Bloomington; Indianapolis, pp. 29–55.
. In: , , pp.
Morgan, Gary S., Thompson, M.E., Hester, P.M., 2007. A Pliocene camel trackway near Santa Fe, New Mexico. Bull. N. M.Mus. Nat. Hist. Sci. 42, 315–318.
Petti, F.M., Avanzini, M., Belvedere, M., De Gasperi, M., Ferretti, P., Girardi, S., Remondino, F., Tomasoni, R., 2008. Digital 3D modeling of dinosaur footprints by photogrammetry and laser scanning techniques: integrated approach at the Coste dell' Anglone tracksite (lower Jurassic, Southern Alps, Northern Italy). Acta Geol. 83, 303–315.
Pond, S., Lockley, M.G., Lockwood, J., Breithaupt, B.H., Matthews, N.A., 2014. Tracking Dinosaurs on the Isle of Wight: a review of tracks, sites, and current research. Biol. J. Linn. Soc. 113, 737–757. https://doi.org/10.1111/bij.12340757.
Raber, G.T., Jensen, J.R., Schill, S.R., Schuckman, K., 2002. Creation of digital terrain models using an adaptive vegetation point removal process. Photogramm. Eng. Rem. Sens. 68, 1307–1315.
Raichlen, D.A., Gordon, A.D., Harcourt-Smith, W.E.H., Foster, A.D., Haas, W.R., 2010. Laetoli footprints preserve earliest direct evidence of human-like bipedal biomechanics. PLoS One 5, e9769.
Roach, N.T., Hatala, K.G., Ostrofsky, K.R., Villmoare, B., Reeves, J.S., Du, A., Braun, D.R., Harris, J.W.K., Behrensmeyer, A.K., Richmond, B.G., 2016. Pleistocene footprints show intensive use of lake margin habitats by Homo erectus groups. Sci. Rep. 6, 26374.
Roberts, D.L., 2008. Last interglacial hominid and associated vertebrate fossil trackways in coastal eolianites, South Africa. Ichnos 15, 190–207.
Rüther, H., Smit, J., Kamamba, D., 2012. A comparison of close-range photogrammetry to terrestrial laser scanning for heritage documentation. S. Afr. J. Geol. 1, 1–14.

Ružić, I., Marović, I., Čedomir, B., Ilić, S., 2014. Coastal cliff geometry derived from structure-from- motion photogrammetry at Stara Baška, Krk Island Croatia. Geo Mar. Lett. 34, 555–565. https://doi.org/10.1007/s00367-014-0380-4.

Salvi, J., Matabosch, C., Fofi, D., Forest, J., 2007. A review of recent range image registration methods with accuracy evaluation. Image Vis Comput. 25, 578–596.

Schmincke, H.-U., Kutterolf, S., Perez, W., Rausch, J., Freundt, A., Staunch, W., 2009. Walking through volcanic mud: the 2,100 year old Acahualinca footprints (Nicarauga) I: stratigraphy, lithology, volcanology and the age of the Acahualinca section. Bull. Volcanol. 71, 479–493. https://doi.org/10.1007/s00445-008-235-9.

, .

Stern, J.T., Susman, R.L., 1983. The locomotor anatomy of Australopithecus afarensis. Am. J. Phys. Anthropol. 60, 279–317.

Stumpf, A., Malet, J.-P., Allemand, P., Pierrot-Deseilligny, M., Skupinski, G., 2015. Ground-based multi-view photogrammetry for the monitoring of landslide deformation and erosion. Geomorphology 231, 130–145. https://doi.org/10.1016/j.geomorph.2014.10.039.

Wackrow, R., Chandler, J.H., 2011. Minimising systematic error surfaces in digital elevation models using oblique convergent imagery. Photogramm. Rec. 26, 16–31. https://doi.org/10.1111/j.1477-9730.2011.00623.x.

Warrick, J.A., Ritchie, A.C., Adelman, G., Adelman, K., Limber, P.W., 2017. New techniques to measure cliff change from historical oblique aerial photographs and Structure-from-Motion photogrammetry. J. Coast Res. 33, 39–55, DOI:10.2112J-COASTRES-D-16-00095.1.

Wenzel, K., Rothermel, M., Fritsch, D., Haala, N., 2013. Image acquisition and model selection for multi- view stereo. Int. Arch. Photogrammetry Remote Sens. Spatial Inf. Sci. 251–258 https://doi.org/10.5194/isprsarchives-XL-5-W1-251-2013.

Westoby, M.J., Brasington, J., Glasser, N.F., Hambrey, M.J., Reynolds, J.M., 2012. Structure-from- Motion' photogrammetry: a low-cost, effective tool for geoscience applications. Geomorphology 179, 300–314. https://doi.org/10.1016/j.geomorph.2012.08.021.

White, T.D., 1980. Evolutionary implications of Pliocene hominid footprints. Science 208, 175–176.

Wiseman, A., De Groote, I., 2018. A three-dimensional geometric morphometric study of the effects of erosion on the morphologies of modern and prehistoric footprints. J. Archaeol. Sci.: Report 17, 93–102. https://doi.org/10.1016/j.jarep.2017.10.044.